SAND2022-3462J

AIP Advances

A discussion on various experimental methods of impact ionization coefficient measurement in GaN

Dong Ji[1,2], Ke Zeng[2], Zhengliang Bian[2], Bhawani Shankar[2], Brendan P. Gunning[3], Andrew Binder[3], Jeramy R. Dickerson[3], Ozgur Aktas[4], Travis J. Anderson[5], Robert J. Kaplar[3], Srabanti Chowdhury[2]

1. The Chinese University of Hong Kong, Shenzhen, China.

2. Stanford University, Stanford, CA, USA

3. Sandia National Laboratory, Albuquerque, NM, USA

4. Edynx, Inc., Pleasanton, CA, USA

5. Naval Research Laboratory, Washington, DC, USA

Corresponding authors: jidong@cuhk.edu.cn and srabanti@stanford.edu

Abstract

Impact ionization coefficients play a critical role in semiconductors. In addition to silicon, silicon carbide and gallium nitride are important semiconductors that are being seen more as mainstream semiconductor technologies. As a reflection of the maturity of these semiconductors, predictive modeling has become essential to device and circuit designers, and impact ionization coefficients play a key role here. Recently, several studies have measured impact ionization coefficients. We dedicated the first part of our study to comparing three experimental methods to estimate impact ionization coefficients in GaN, which are all based on photomultiplications but feature characteristic differences. The first method inserts an InGaN hole-injection layer, the accuracy of which is challenged by the dominance of ionization in InGaN, leading to possible overestimation of the coefficients. The second method utilizes the Franz-Keldysh effect for hole injection but not for electrons, where the mixed injection of induced carriers would require a margin of error. The third method uses complementary p-n and n-p structures that have been at the basis of this estimation in Si and SiC and leans on the assumption of a constant electric field, any deviation would require a margin of error. In the second part of our study, we evaluated the models using recent experimental data from diodes demonstrating avalanche breakdown.

Introduction

Electron and hole impact ionization coefficients are critical parameters in the design of high field applications of semiconductors, such as impact ionization avalanche transit-time (IMPATT) diodes, avalanche photodiodes (APDs), and power switches [1]. Impact ionization in gallium nitride (GaN) is a topic of obvious interest because the material is a forerunner of that used in many high-power applications. Avalanche breakdown in GaN power diodes was first reported in 2013 on a p-n junction fabricated on free-standing substrates [2]. Since then, there have been several other studies on it and showing impact ionization coefficient measurements [3–20]. Other avalanche-based devices, such as IMPATT diodes and APDs, have also been reported [21–28].

Researchers began to measure impact ionization coefficients in GaN in the 1990s. In 1999, Kunihiro *et al*. first reported an electron's impact ionization in GaN using lateral AlGaN/GaN test structures grown on a sapphire substrate [29]. Those authors extracted the electron's impact ionization coefficient using a gate-current analysis of AlGaN/GaN HEMT. In 2006, Tut *et al*. measured impact ionization coefficients in $Al_xGa_{1-x}N$ based on an APD structure grown on sapphire, adopting a photomultiplication method [30]. In 2012, Ozbek *et al*. reported impact ionization coefficient measurements using an electron beam-induced current technique in a Schottky diode grown on both sapphire and free standing GaN substrates [31]. These early studies, conducted with the best possible GaN structures, did not confirm the avalanching phenomenon but set the stage for future work. No conclusive avalanche, supported by the positive temperature coefficient of the breakdown voltage, was reported until 2013, when Avogy Inc. demonstrated their 2600 V vertical GaN p-n diodes grown on free-standing GaN substrates [2]. Multiple studies since that time have found avalanche breakdown in GaN p-n diodes based on free-standing GaN substrates. Following the availability of avalanching diodes, attempts to measure impact ionization coefficients have been made and reported [9, 11, 15–17], and are ongoing. The impact ionization coefficient sheds light on the performance limits of GaN for power devices [32]. However, a critical analysis of these methods is both interesting and important. Because none of these measurement methods are direct, it is to be expected that each will have its own sources of error. In this paper, we explored and compared these methods.

One of the methods examined is based on photomultiplication, a standard technique that is used in Si, GaAs, and SiC for impact ionization measurements and that has been implemented in GaN as well [33–36]. The two key criteria for impact ionization studies conducted using

photomultiplication methods in Si and SiC are: 1) the device should exhibit a robust avalanche breakdown, and 2) the electrons and holes should be separately injected so that the electron and hole impact ionization coefficients can be extracted separately. Thanks to the high-quality epitaxial growth on high-quality freestanding substrates, a robust avalanche breakdown in the GaN p-n junction is now routinely possible, satisfying the first criterion. However, creating separate electron and hole injection is the key challenge in the measurement of the impact ionization coefficients.

The photomultiplication method uses light with a photon energy that is larger than the bandgap of a semiconductor to create electron-hole pairs, where only photon-excited electrons are injected to the drift region when the anode region is illuminated (p-GaN), and only photon-excited holes are injected into the drift region when illuminating on the cathode region (n-GaN). The structure used in the photomultiplication method can be either a single p-n diode or complementary p-n diodes, as shown in Fig. 1. Fig. 1(a) shows electron and hole injection in the same device structure, where part of the substrate must be removed to enable hole injection via back illumination. Fig. 1(b) shows the electron and hole injection in complementary device structures, where both electron and hole injections are triggered by top illumination. However, neither method is easy to establish. The substrate removal technique suffers from various mechanical stress issues, and p-GaN substrates are not readily available. This prompted exploration of other techniques that can be used to apply the photomultiplication method to GaN.

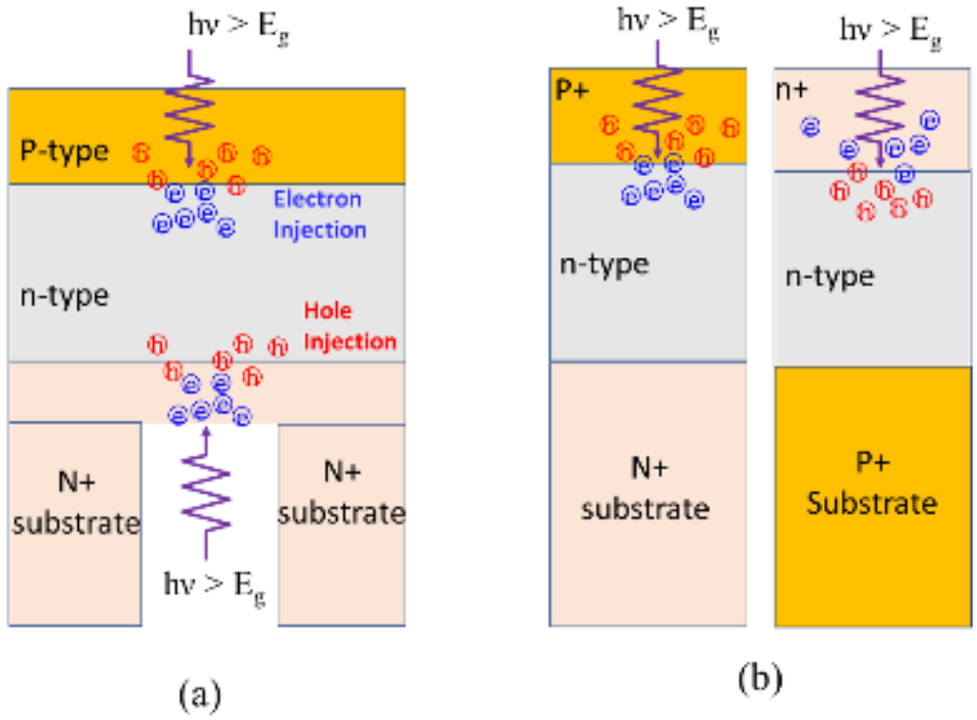

Figure 1. (a) Creating electron and hole injections using a single device structure; (b) creating electron and hole injection using separate device structures.

Discussion of different methods

In 2012, Ozbek *et al*. reported impact ionization coefficients in bulk GaN using a Schottky diode [31], as shown in Fig. 2. An electron beam was used to excite both electrons and holes inside the low-doped drift region. With the help of TCAD simulation, Ozbek *et al*. found that the impact ionization coefficients of the electron and hole could be separately extracted by changing the depth (t_{ex}) of excitation. When t_{ex} is less than 50 nm, the impact ionization coefficient of the electron could be extracted, while the hole coefficient was required t_{ex} to be larger than 300 nm. The electron beams excited both electrons and holes inside the drift region, particularly where the excitation depth was large, which therefore could not enable the separation of the impact ionization coefficients of electrons and holes.

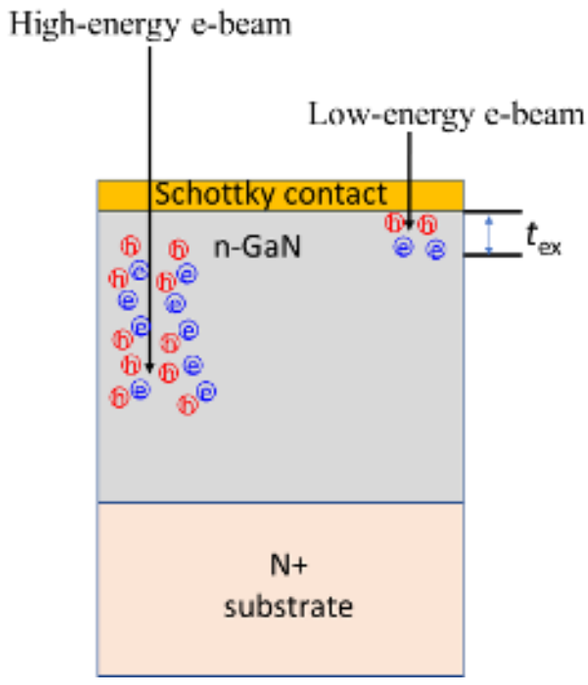

Figure 2. The GaN-on-GaN Schottky diode used in the electron beam-induced multiplication method [31].

In 2018, Cao *et al*. reported the impact ionization coefficients in bulk GaN using the GaN/$In_{0.07}Ga_{0.93}N$/GaN heterostructures, as shown in Fig. 3 [11]. A photomultiplication method was adopted, where a 310 nm UV light source, whose photon energy is larger than the bandgap of GaN, was used to illuminate the GaN/$In_{0.07}Ga_{0.93}N$/GaN structure. Because the absorption coefficient of the 310 nm light in GaN is 1.25×10^5 cm^{-1} [37], the light could not penetrate the top layer of p-GaN, resulting in electron injection into the reverse-biased p-n junction. For hole injection, a 390 nm UV light, with a photon energy that is less than the bandgap of GaN but larger than the bandgap of the inserted $In_{0.07}Ga_{0.93}N$ layer, was used to illuminate the device. Most of the light penetrated the top layers of the GaN and reached the $In_{0.07}Ga_{0.93}N$ layer, exciting electron-hole pairs inside the $In_{0.07}Ga_{0.93}N$ layer. Due to the presence of an electric field in the depleted region, the holes moved toward the anode region, while the electrons traveled toward the cathode region, thereby creating a hole injection in the GaN drift region, as shown in Fig. 3. This method separated electron and hole injections, but there are certain limitations of this method that are discussed here. First, it could be argued that the presence of a 80 nm $In_{0.07}Ga_{0.93}N$ layer might have

affected the material quality of the top GaN p-n junction due to the lattice mismatch between $In_{0.07}Ga_{0.93}N$ and GaN. Second, as the 80 nm $In_{0.07}Ga_{0.93}N$ layer was undoped, the electric field remained constant in the $In_{0.07}Ga_{0.93}N$ layer and induced impact ionization inside the $In_{0.07}Ga_{0.93}N$ layer. Where the 80 nm of $In_{0.07}Ga_{0.93}N$ was not relaxed, the presence of the polar charge induced by the piezoelectric effect made the case more difficult by keeping the electric field high in the $In_{0.07}Ga_{0.93}N$ layer. This implies that the impact ionization coefficients of $In_{0.07}Ga_{0.93}N$ were more likely to be extracted, rather than those of GaN. The distribution of the electric field is shown in Fig. 4, where the differences in the peak amplitudes of the electric field inside GaN and $In_{0.07}Ga_{0.93}N$ are around 0.1 MV/cm. The bandgap of the $In_{0.07}Ga_{0.93}N$ is 3.24 eV [38], which is less than the value for GaN, namely 3.5 eV. According to a previous study [39], the empirical expression for the critical electric field based solely on bandgap values can be written as

$$E_C = 1.73 \times 10^5 (E_G)^{2.5} \qquad (1)$$

The critical field in $In_{0.07}Ga_{0.93}N$, $E_{C,InGaN}$, is thus around 82% of $E_{C,GaN}$. Therefore, there is a high probability that the impact ionization occurred inside the $In_{0.07}Ga_{0.93}N$ rather than GaN.

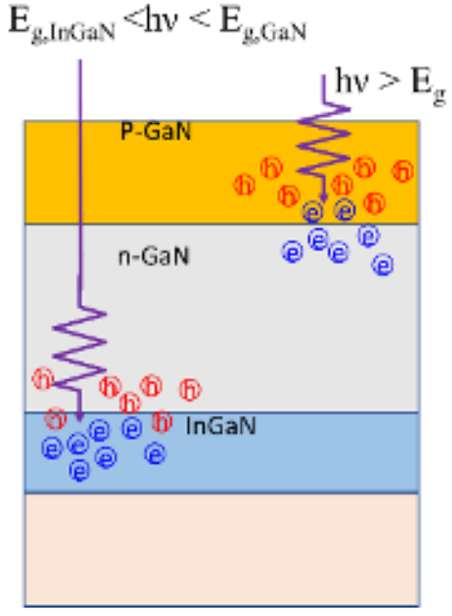

Figure 3. Schematic of the photomultiplication method adopted by Cao *et al*. [11].

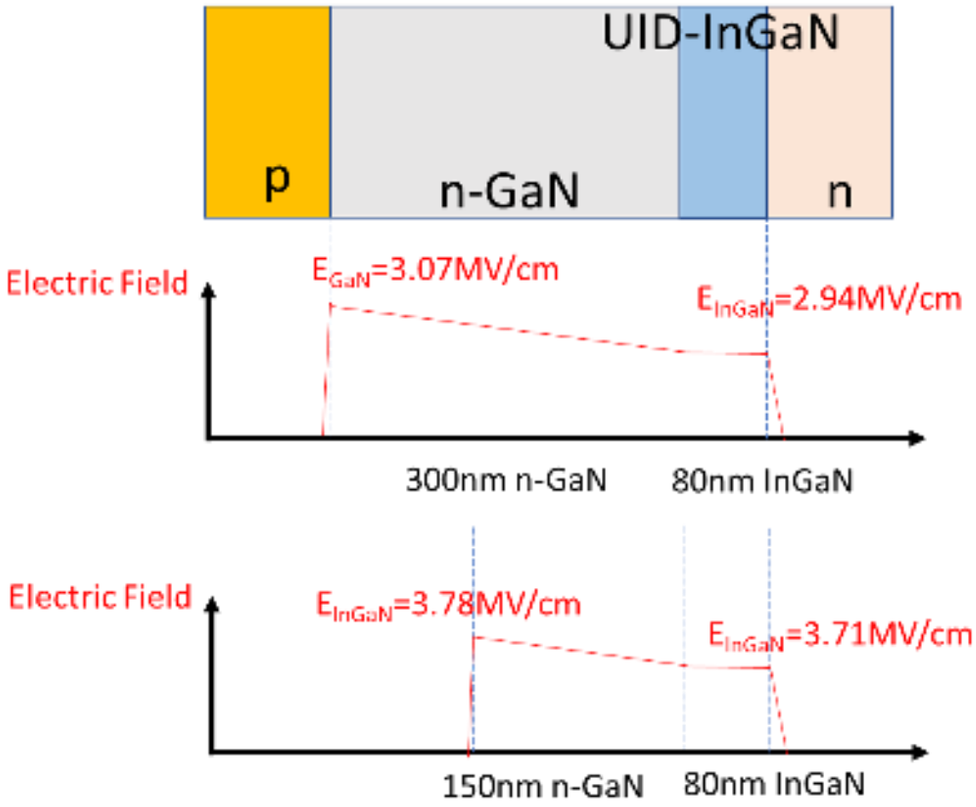

Figure 4. Electric field distribution inside the depleted region when the devices are reverse-biased. The polarization field is not included.

In 2019, Maeda *et al*. reported an impact ionization coefficient measurement using a similar photomultiplication method [15, 16]. However, it was assumed that the electron and hole had the same impact ionization coefficient ($\alpha = \beta$) and the authors did not try to separate the electron- and hole-initiated impact ionization. This assumption, although it is often used in Si, is an oversimplification in GaN because the unique energy band diagram leads to a significant difference in the effective masses of the electron and hole, which in turn leads to a large difference in their impact ionization coefficients in GaN that cannot be ignored. Nonetheless, it adds value to this discussion and leads to improved methods.

In 2020, Maeda *et al*. improved on their former methods by separating the electron- and hole-initiated impact ionization [17]. Maeda *et al*. utilized the Franz-Keldysh effect for hole injection, as shown in Fig. 5(a). The Franz-Keldysh effect describes how the absorption threshold of a

semiconductor can shift to lower photon energies when an external electric field is applied, as shown in Fig. 5(b). The intrinsic GaN has a threshold absorption photon energy of around 3.5 eV, while the absorption thresholds of photon energy shift to 3.3 eV and 3.2 eV, respectively, when 1 MV/cm and 2 MV/cm external electric fields are present in GaN. Although the Franz-Keldysh effect can create hole injection using light with lower photon energy, more than 80% of the carriers are generated inside the depletion region, and only 20% are generated in the first 50 nm region close to the p-n junction interface, as shown in Fig. 5(c). This creates a mixed-injection issue for impact ionization coefficient measurement, with the possibility of some errors in the result, as discussed in a previous study [40].

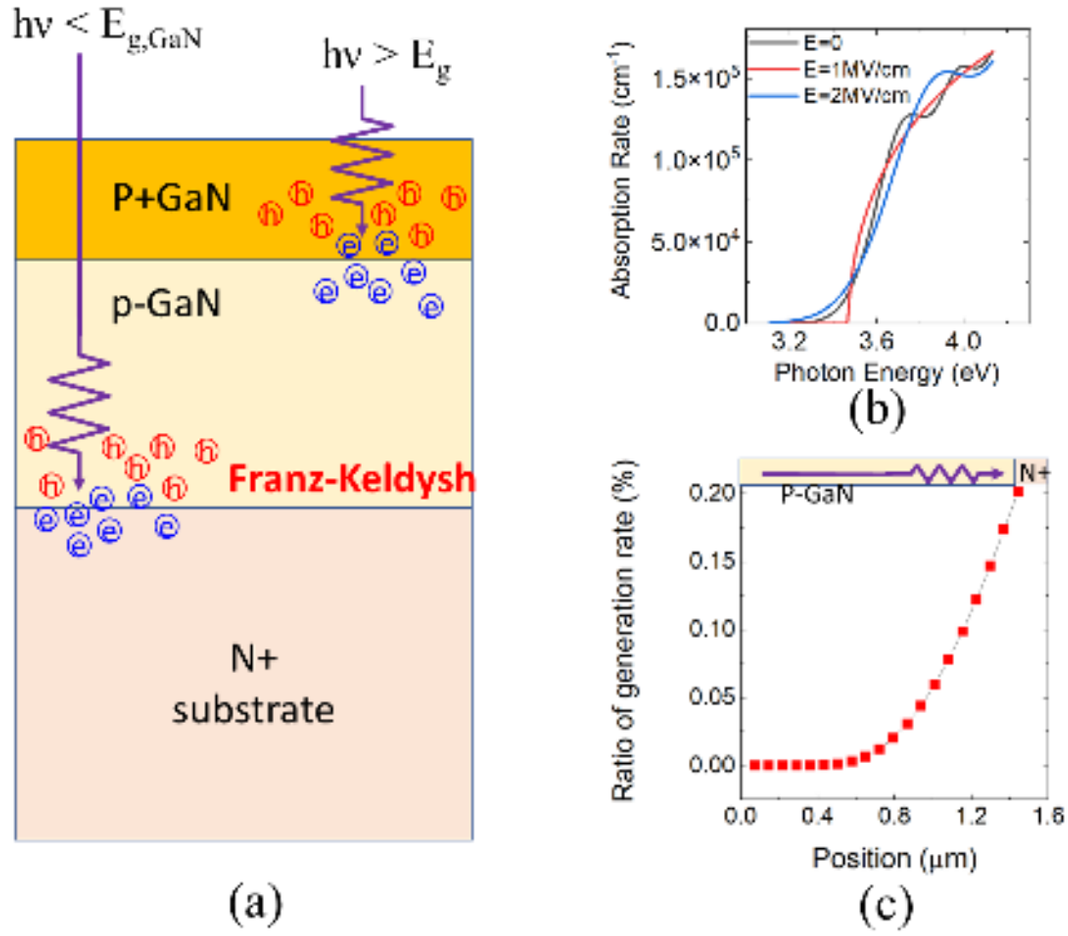

Figure 5. (a) Schematic of the p-n structure used in Franz-Keldysh-induced photomultiplication methods; (b) the absorption rate of GaN under a different external electric field of 0 MV/cm, 1

MV/cm, and 2 MV/cm; and (c) the generation rate along the depletion region, indicating 20% generation in the first 50 nm depletion region close to the interface.

According to the theorization of the Franz-Keldysh effect, the absorption coefficient under an electric field (E) is given by:

$$\alpha(\omega, E) = \frac{e^2|\boldsymbol{e}\cdot\boldsymbol{p_{cv}}|^2}{2\varepsilon_0 m_0^2 nc\omega}\left(\frac{8\mu_{\parallel}\mu_{\perp}}{\hbar^3}\right)^{1/2} \times \sqrt{\hbar\theta}\left[Ai'^2(\eta) - \eta Ai^2(\eta)\right], \qquad (2)$$

where $\mu_{\parallel} = \frac{m_e^{\parallel} m_h^{\parallel}}{m_e^{\parallel}+m_h^{\parallel}}$, $\mu_{\perp} = \frac{m_e^{\perp} m_h^{\perp}}{m_e^{\perp}+m_h^{\perp}}$, $\eta = \frac{E_g - h\nu}{\hbar\theta}$, $\hbar\theta = \left(\frac{e^2\hbar^2E^2}{2\mu_{\parallel}}\right)^{1/3}$.

The accurate prediction of Franz-Keldysh-induced absorption depends on the accuracy of several material parameters, including the momentum matrix element $|\boldsymbol{e}\cdot\boldsymbol{p_{cv}}|$, the refractive index n, and the reduced effective mass $\mu_{\parallel}$ and $\mu_{\perp}$. However, no data have been reported for $|\boldsymbol{e}\cdot\boldsymbol{p_{cv}}|$ in GaN. Furthermore, there is variation in $\mu_{\parallel}$ and $\mu_{\perp}$ [41–44]. Maeda *et al.*'s analysis [17] fits the absorption rate in GaN under E=0 V/cm reported by Muth *et al*. [37], and roughly obtains the value of $|\boldsymbol{e}\cdot\boldsymbol{p_{cv}}|$. However, due to the nonlinear relationship between the absorption coefficient and the electric field, the fitting curve in the zero electric field and low electric field regions predict the absorption coefficient in the high electric field region and may have some errors. To validate this statement, the Franz-Keldysh-induced photocurrent was determined using the absorption coefficient as a function of voltage and is plotted in Fig. 6. When the applied voltage is lower than 50 V, by varying the reduced effective mass from 0.14 m_0 to 0.2 m_0, no obvious difference appears among the calculated photocurrents, and all of the calculated photocurrents match to the measured data. However, when the applied voltage is higher, e.g., 200 V, the variation among the calculated photocurrent is four times as large, which leads to an error bar of 4× in the extracted avalanche multiplication, whose value can be obtained using the measured photocurrent divided by the calculated photocurrent induced by the Franz-Keldysh effect.

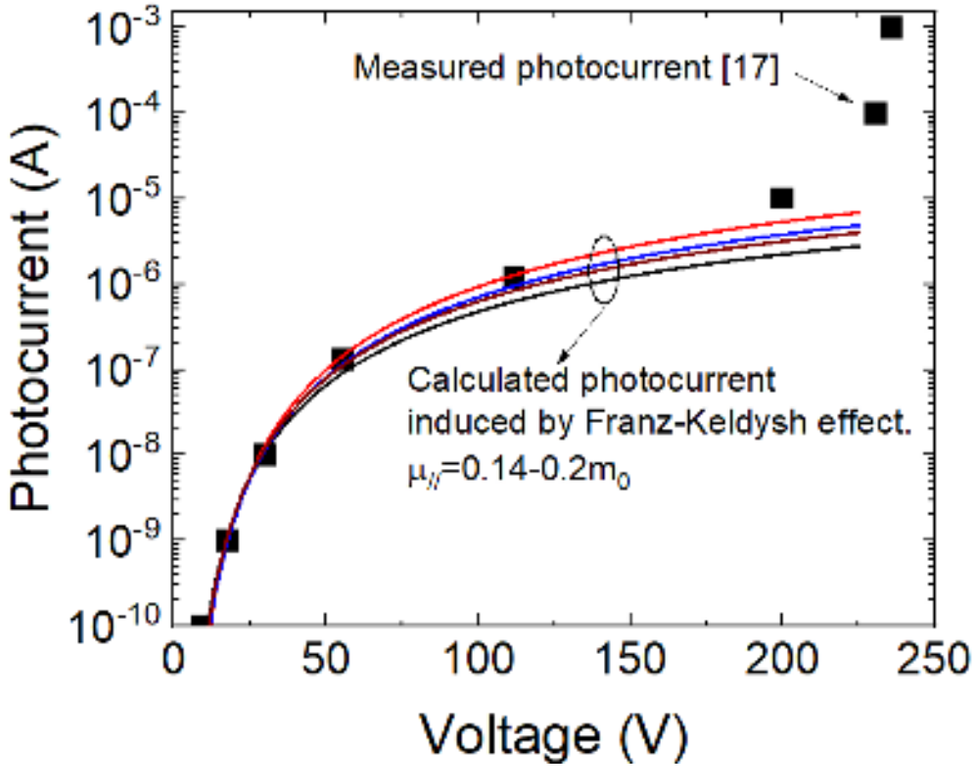

Figure 6. Franz-Keldysh-induced photocurrent as a function of applied voltage.

In 2019, we reported an impact ionization coefficient study using the structures shown in Fig. 7 [9]. We used a modified structure that resembles the concept given in Fig. 1(b). Both p-n and n-p structures were fabricated and used for coefficient extraction of the impact ionization. The n-p structure with buried p-GaN layer is challenging because of the formation of the Mg-H complex during the material growth, and it is difficult to activate the acceptors by breaking the complex and driving out hydrogen. We employed a method involving doping and activation that rendered the highly doped p contact layer conductive and compensated for the high field region. The substantial activation of Mg in the buried structure was verified with a combination of SIMS and p-contact layer resistivity measurements [9]. This allowed us to adopt the widely used photomultiplication method in Si, GaAs, and SiC [33–36]. A light that has a photon energy larger than the energy bandgap of a semiconductor was used to illuminate the top layers of the p-n and n-p structures, creating electron and hole injections into the drift regions. The multiplication factor can be obtained by comparing the photocurrent with impact ionization and the initial photocurrent without

impact ionization. In our study, hole-initiated multiplication occurred when the electric field reached 2 MV/cm, while the electron-initiated multiplication occurred when the electric field reached over 3 MV/cm, indicating that the ratio of the hole's impact ionization coefficient over the electron's is quite large when the electric field is relatively low (2 MV/cm to 2.5 MV/cm); therefore, an electron's impact ionization can be negligible at a relatively low electric field, which can simplify the calculation. A similar strategy can be observed in Niwa *et al.*'s study of SiC [35] and Cao *et al.*'s study of GaN [12]. In our study, an n-p structure with a 1.2 µm thick, low-doped ([Si] = ~1 × 10^{16} cm^{-3}, [Mg] dopants were compensated) drift region was fabricated for the hole's impact ionization coefficient extraction. By solving the Poisson equation when a voltage of 315 V was applied, we found that the electric field along the drift region was almost constant, with a variation of less than 10%; therefore, a uniform electric field distribution was assumed across the drift region during the calculation. The same simplification was also adopted in two previous studies [12, 35].

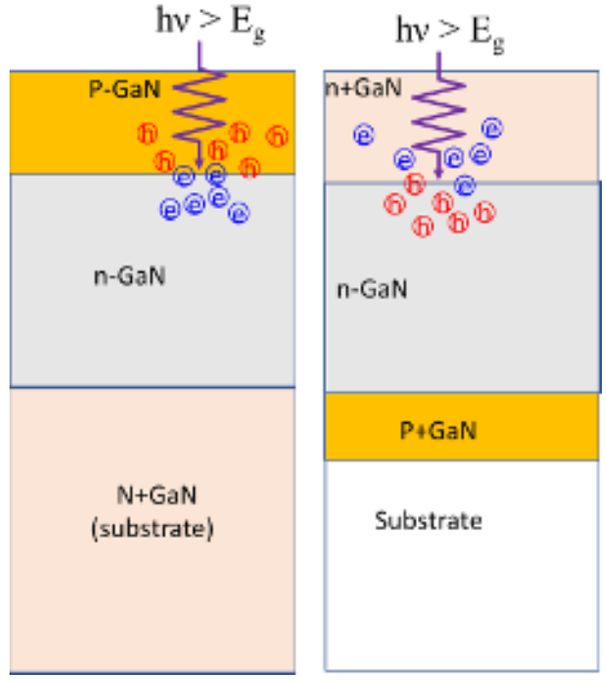

Figure 7. The p-n and n-p structures used for impact ionization coefficient study by Ji et al. [9].

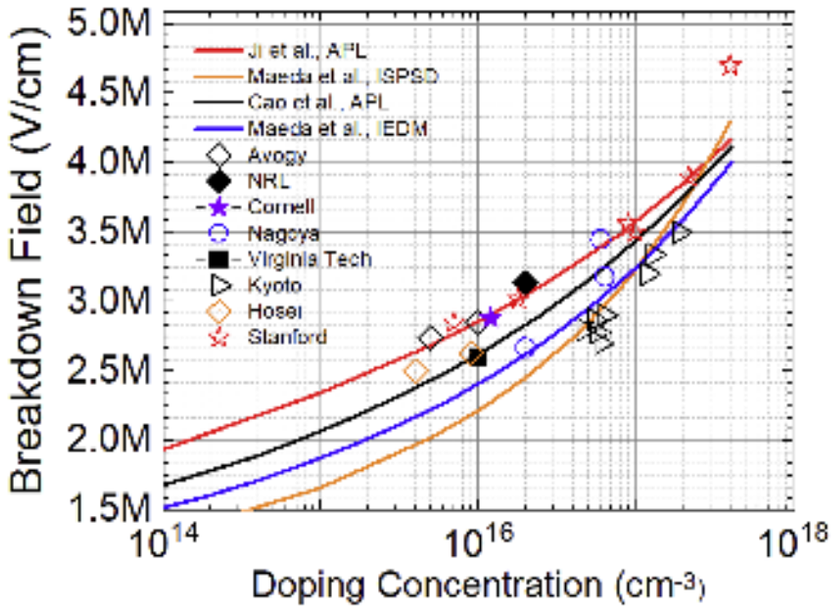

Fig. 8. Projected and experimental breakdown electric field as a function of doping concentration in the non-punch through structures. Experimental data are all from non-punch through structures [3-17].

Discussion of experimental breakdown fields

After this discussion and comparison of various methods of impact ionization extraction, it would be interesting to identify how far various measured critical breakdown electric fields agree with the models, observing that every method has its own limitations. One exercise that has proved beneficial in other examinations of semiconductor technologies involves collecting various device data and overlaying on the projected values obtained using various impact ionization coefficients. We performed a similar study in GaN. By solving the impact ionization integration equations (Eqs. 3 and 4) in the non-punch through structures, we obtained the breakdown electric field as a function of the doping concentration [8, 12, 32, 45].

$$1-\frac{1}{M_p}=\int_0^W \beta e^{-\int_0^x(\beta-\alpha)dx'}dx \quad (3)$$

and

$$1-\frac{1}{M_n}=\int_0^W \alpha e^{-\int_x^W(\alpha-\beta)dx'}dx, \quad (4)$$

where α and β are the impact ionization coefficients of the electron and hole, M_p and M_n are hole- and electron-initiated avalanche multiplication factors, and $W = \frac{E_C \varepsilon}{qN_D}$ is the width of the depletion region.

The solid curves in Fig. 8 indicate the projected breakdown electric field using various reported impact ionization coefficients [9, 11, 16, 17]. The different symbols indicate the experimental data reported by various groups [3–17]. It is critical to note that only data from devices demonstrating an avalanche were collected. For different impact ionization coefficients, the projected breakdown electric field as a function of doping concentration were plotted and compared to the reported experimental data, including our own data.

The curves shown in the above figure indicate non-punch through drift region design, whose electric field distribution is triangular. The peak electric field was assumed to be uniform across the area of the p-n junction. It is important to note that due to the unoptimized edge termination design, the electric field across the p-n junction may not be uniform, which would decrease the breakdown voltage and the extracted average breakdown electric field as well. We therefore would argue that an even higher critical electric field is to be expected in GaN when uniform avalanche is achieved.

Typically, when the carriers' multiplication factor M reaches 100, this indicates that the avalanche breakdown occurs in the device [46,47]. M is proportional to the product of the thickness of the drift region and the electric field. In power devices, the design of drift region doping and thickness are critical for the device breakdown. A special case is that of the device with a punch-through drift region design. If the doping concentration is constant, in the punch-through drift region design, the drift region is thinner than the non-punch-through case, and the electric field across the device is a trapezoid, which differs from the triangular-shaped electric field distribution in the non-punch-through design. Because the punch-through design has a thinner drift region, it requires a greater electric field to trigger the carriers' multiplication, and this is not included in Fig. 8.

An element to be taken into account in the calculation of GaN's impact ionization coefficients and critical breakdown of the electric field is the role of the relative dielectric constant, ε_r. There are three relative dielectric constant values that are widely used in the literature, 8.9 [48–55], 9.5 [56], and 10.4 [57]. In the aforementioned methods, due to the assumption of a constant electric field,

differences in ε_r do not impact the hole's impact ionization coefficient [9, 11]. Although the value of ε_r affected the peak electric field calculation in two previous studies with respect to the electron impact ionization coefficient [9, 11], the impact was not significant. The electric field in a non-punch-through p-n structure can be written as

$$E_{peak} = \sqrt{\frac{2V_{br}qN_d}{\varepsilon_r\varepsilon_0}}. \quad (5)$$

The peak electric field variation, $\delta E_{peak}/E_{peak}$, caused by different ε_r values, can be less than 8%, so it is not the main reason for the significant difference in the three studies noted above.

Conclusion

We investigated different experimental methods of estimating the impact ionization coefficients that have been recently used in GaN. The three main methods were as follows: Method 1, photomultiplication with a InGaN insert hole-injection layer; Method 2, photomultiplication with the Franz-Keldysh effect for hole injection; and Method 3, photomultiplication in p-n and n-p structures. In Method 1, our analysis suggests that the impact ionization may have occurred inside the InGaN layer; therefore, the extracted impact ionization coefficients belong to InGaN, rather than GaN, which may produce an underestimation of the critical electric field in GaN. In Method 2, we suggest that because more than 80% of the carriers are generated inside the material, the distributed mixed injection could lead to errors in the extraction of both the electron and hole's impact ionization coefficients. Moreover, the Franz-Keldysh effect has a mathematical formulation that depends on multiple parameters. The values of these parameters must be accurate or determined in multiple experiments. Any variation in these parameters could lead to additional errors. In Method 3, a n-p structure with a 1.2 μm thick low-doped ([Si] = ~1×10^{16} cm^{-3}) drift region was fabricated for the hole's impact ionization coefficient extraction. To simplify the calculation, it was assumed that the electron's impact ionization coefficient is negligible compared to the hole when the electric field was less than 2.5 MV/cm, and the electric field across the drift region was assumed to be constant. It is worth noting that these mathematical simplifications were also used in other studies as well [12, 35]. A comparison of the results in Ref. 12 to those in Ref. 11, where no simplification was assumed, found no obvious effects on the results. Finally,

experimental breakdown fields were plotted from reports on various non-punch-through methods showing avalanche against modeled data to offer a view of the evolution of this discussion. As more data are gathered, these models can be tried and tested further, and their accuracy will be determined over time.

The work is supported by ARPA-E SWITCHES program. Sandia National Laboratories is a multi-mission laboratory managed and operated by National Technology & Engineering Solutions of Sandia, LLC, a wholly owned subsidiary of Honeywell International Inc., for the U.S. Department of Energy's National Nuclear Security Administration under contract DE-NA0003525. The views expressed in this article do not necessarily represent the views of the U.S. Department of Energy or the U.S. Government

Figure captions

Figure 1. (a) Creating electron and hole injections using a single device structure; (b) creating electron and hole injection using separate device structures.

Figure 2. The GaN-on-GaN Schottky diode used in the electron beam-induced multiplication method [31].

Figure 3. Schematic of the photomultiplication method adopted by Cao *et al*. [11].

Figure 4. Electric field distribution inside the depleted region when the devices are reverse-biased. The polarization field is not included.

Figure 5. (a) Schematic of the p-n structure used in Franz-Keldysh-induced photomultiplication methods; (b) the absorption rate of GaN under a different external electric field of 0 MV/cm, 1 MV/cm, and 2 MV/cm; and (c) the generation rate along the depletion region, indicating 20% generation in the first 50 nm depletion region close to the interface.

Figure 6. Franz-Keldysh-induced photocurrent as a function of applied voltage.

Figure 7. The p-n and n-p structures used for impact ionization coefficient study by Ji et al. [9].

Fig. 8. Projected and experimental breakdown electric field as a function of doping concentration in the non-punch through structures. Experimental data are all from non-punch through structures [3-17].

Reference

[1] J. Baliga, *Fundamental of Power Semiconductor Devices* (Springer Science + Business Media, LLC, New York, NY, US 2008) p. 91.

[2] D. Disney, H. Nie, A. Edwards et al., in *Proceedings of the 25th International Symposium on Power Semiconductor Devices & ICs*, Kanazawa, Japan, 26-30 May 2013, pp. 59-62.

[3] K. Nomoto, B. Song, Z. Hu, M. Zhu, M. Qi, N. Kaneda, T. Mishima, T. Nakamura, D. Jena, and H. G. Xing, IEEE Electron Device Letters, 37, 161 (2016).

[4] H. Fukushima, S. Usami, M. Ogura, Y. Ando, A. Tanaka, M. Deki, M. Kushimoto, S. Nitta, Y. Honda and H. Amano, Japanese Journal of Applied Physics, 12, SCCD25 (2019).

[5] H. Ohta, N. Asai, F. Horikiri, Y. Narita, T. Yoshida, and T. Mishima, Japanese Journal of Applied Physics, 58, SCCD03, (2019).

[6] J. Liu, M. Xiao, R. Zhang, S. Pidaparthi, C. Drowley, L. Baubutr, A. Edwards, H. Cui, C. Coles, and Y. Zhang, IEEE Electron Device Lett., 41, 1328 (2020).

[7] D. Ji, S. Li, B. Ercan, C. Ren, and S. Chowdhury, IEEE Electron Device Letters, 41, 264 (2020).

[8] D. Ji and S. Chowdhury, Appl. Phys. Lett., 117, 252107 (2020).

[9] D. Ji, B. Ercan, and S. Chowdhury, Appl. Phys. Lett., 115, 073503 (2019).

[10] D. Ji, B. Ercan, G. Benson, A. Newaz, and S. Chowdhury, in *Proceedings of IEEE International Reliability Physics Symposiums*, Dalla, TX, USA, 28 April-30 May 2020, pp. 1-4.

[11] L. Cao, H. Ye, J. Wang, and P. Fay, Appl. Phys. Lett., 112, 262103 (2018).

[12] L. Cao, Z. Zhu, G. Harden, H. Ye, J. Wang, A. Hoffman, and P. J. Fay, IEEE Transactions on Electron Devices, 68, 1228 (2021).

[13] L. Cao, H. Ye, J. Wang, and P. Fay, Physica Status Solidi (b), 257, 1900373 (2020).

[14] T. Maeda, T. Narita, H. Ueda, M. Kanechika, T. Uesugi, T. Kachi, T. Kimoto, M. Horita, and J. Suda, in *Proceedings of IEEE International Electron Devices Meeting*, San Francisco, CA, USA, 1-5, Dec. 2018, pp. 689-693.

[15] T. Maeda, T. Narita, H. Ueda, M. Kanechika, T. Uesugi, T. Kachi, T. Kimoto, M. Horita, and J. Suda, Appl. Phys. Lett. 115, 142101 (2019).

[16] T. Maeda, T. Narita, H. Ueda, M. Kanechika, T. Uesugi, T. Kachi, T. Kimoto, M. Horita, and J. Suda, in *Proceedings of 31st International Symposium on Power Semiconductor Devices and ICs*, Shanghai, China, 19-23 May 2019, pp.59-62.

[17] T. Maeda, T. Narita, S. Yamada, T. Kachi, T. Kimoto, M. Horita, and J. Suda, in Proceedings of 2019 IEEE International Electron Devices Meeting, San Francisco, CA, USA, 7-11 Dec. 2019, pp. 70-73.

[18] J. Wang, G. Yu, H. Zong, Y. Liao, W. Lu, W. Cai, X. Hu, Y. Xie, and H. Amano, Appl. Phys. Lett. 118, 212102 (2021).

[19] I. C. Kizilyalli, A. P. Wdwards, H. Nie, D. Disney, and D. Bour, IEEE Transactions on Electron Devices, 60, 3067 (2014).

[20] K. Nie, W. Xu, F. Ren, D. Zhou, D. Pan, J. Ye, D. Chen, R. Zhang, Y. Zheng, and H. Lu, IEEE Electron Device Letters, 41, 469 (2020).

[21] D. Ji, B. Ercan, J. Zhuang, L. Gu, J. Rivas-Davila, and S. Chowdhury, in *Proceedings of Device Research Conference*, Columbus, OH, USA, 21-24 June 2020, pp. 1-2.

[22] P. Fay, O. Aktas, D. Bour, and I. Kizilyalli, Electronics Letters, 51, 1009 (2015).

[23] L. Cao, Ph.D. thesis, Notre Dame University, 2020.

[24] S. Kawasaki, Y. Ando, M. Deki, H. Watanabe, A. Tanaka, S. Nitta, Y. Honda, M. Arai, and H. Amano, Appl. Phys. Express, 14, 046501 (2021).

[25] D. Ji, B. Ercan, G. Benson, A. Newaz, and S. Chowdhury, Appl. Phys. Lett., 116, 211102 (2020).

[26] A. K. Sood, J. W. Zeller, Y. R. Puri, R. D. Dupuis, T. Dethprohm, M. Ji, S. Shen, S. Babu, N. K. Dhar, and P. Wijewarnasuriya, International Journal of Engineering Research and Technology, 10 129 (2017).

[27] M-H Ji, H. Jeong, M. Bakhtiary-Noodeh, S. Shen, T. Detchprohm, A. K. Sood, P. P. Ghuman, S. Babu, N. K. Dhar, J. Lewis, and R. D. Dupuis, in *Gallium Nitride Materials and Devices XIV: Proceedings of SPIE*, San Francisco, CA, USA, 1 March 2019, p.1091814.

[28] W. Wang, IEEE Photonics Technology Lett., 32, 1357 (2020).

[29] K. Kunihiro, K. Kasahara, Y. Takahashi, and Y. Ohno, IEEE Electron Device Letters, 20, 608 (1999).

[30] T. Tut, M. Gokkavas, B. Butun, S. Butun, E. Ulker, and E. Ozbay, Appl. Phys. Lett., 89, 183524 (2006).

[31] A. M. Özbek, Ph.D. Dissertation, North Carolina State University, 2012.

[32] J. A. Cooper and D. T. Morisette, IEEE Electron Device Letters, 41, 892 (2020).

[33] R. V. Overstraeten and H. D. Man, Solid-State Electronics, 13, 583 (1970).

[34] C. Grove, R. Ghin, J. P. R. David, and G. J. Rees, IEEE Transactions on Electron Devices, 50, 2027 (2003).

[35] H. Niwa, J. Suda, and T. Kimoto, IEEE Transactions on Electron Devices, 62, 3326 (2015).

[36] W. S. Loh, B. K. Ng, J. S. Ng, S. I. Soloviev, H. Cha, P. M. Sandvik, C. M. Johnson, and J. P. R. David, IEEE Transactions on Electron Devices, 55, 1984 (2008).

[37] J. F. Muth, J. H. Lee, I. K. Shmagin, and R. M. Kolbas, Appl. Phys. Lett. 71, 2572 (1997).

[38] P. G. Moses, and C. G. Van de Walle, Appl. Phys. Lett., 96, 021908 (2010).

[39] J. L Hudgins, G. S. Simin, E. Santi, and M. A. Khan, IEEE Transactions on Power Electronics, 18, 907 (2003).

[40] G. E. Bulman, L. W. Cook, and G. E. Stillman, Solid-State Electronics, 25, 1189 (1982).

[41] G. D. Chen, M. Smith, J. Y. Lin, H. X. Jiang, S. H. Wei, M. A. Khan, and C. J. Sun, Appl. Phys. Lett. 68, 2784 (1996).

[42] T. Maeda, M. Okada, M. Ueno, Y. Yamamoto, M. Horita, and J. Suda, Appl. Phys. Express, 9, 091002 (2016).

[43] M. Suzuki, T. Uenoyama, and A. Yanase, Phys. Rev. B, 52, 8132 (1995).

[44] A. Punya and W. R. L. Lambrecht, Phys. Rev. B, 85, 195147 (2012).

[45] T. Maeda, T. Narita, S. Yamada, T. Kachi, T. Kimoto, M. Horita, and J. Suda, J. Appl. Phys. 129, 185702 (2021).

[46] K. Lee, and K. Yang, IEEE Photonics Technology Letters, 26, 999 (2014).

[47] K. H. Yoon, M. H. Shin and C. Y. Park, J. Korean Physical Society, 45, 936 (2004).

[48] V. Bougrov, M. E. Levinshtein, S. L. Rumyantsev, and A. Zubrilov, in *Properties of Advanced Semiconductor Materials GaN, AlN, InN, BN, SiC, SiGe*, edited by M.E. Levinshtein, S.L. Rumyantsev and M.S. Shur (John Wiley & Sons, Inc., New York, USA, 2001), pp. 1–30.

[49] J. Hu, Y. Zhang, M. Sun, D. Piedra, N. Chowdhury, and T. Palacios, Materials Science in Semiconductor Processing, 78, 75 (2018).

[50] D. Wei, T. Hossain, D. P. Briggs, and J. H. Edgar, ECS Journal of Solid State Science and Technology, 3, 127 (2014).

[51] M. Kim, J.-H. Seo, U. Singisetti, and Z. Ma, Journal of Chemistry C, 5, 8338 (2017).

[52] K. Zeng, and S. Chowdhury, IEEE Transactions on Electron Devices, 67, 2457 (2020).

[53] Y. Zhang, Z. Chen, W. Li, A. R. Arehart, S. A. Ringel, and H. Zhao, Physica Status Solidi (a), 218, 2000469 (2021).

[54] T. Suemitsu and I. Makabe, Physica Status Solidi (b), 257, 1900528 (2020).

[55] O. Ambacher, J. Smart, J. R. Shealy, N. G. Weimann, K. Chu, M. Murphy, W. J. Schaff, and L. F. Eastman, J. Appl. Phys. 85, 3222 (1999).

[56] O. Ambacher, B. Foutz, J. Smart, J. R. Shealy, N. G. Weimann, K. Chu, M. Murphy, A. J. Sierakowski, W. J. Schaff, and L. F. Eastman, J. Appl. Phys. 87, 334 (2000).

[57] A. S. Barker, Jr. and M. Ilegems, Phys. Rev. B, 7, 743 (1973).

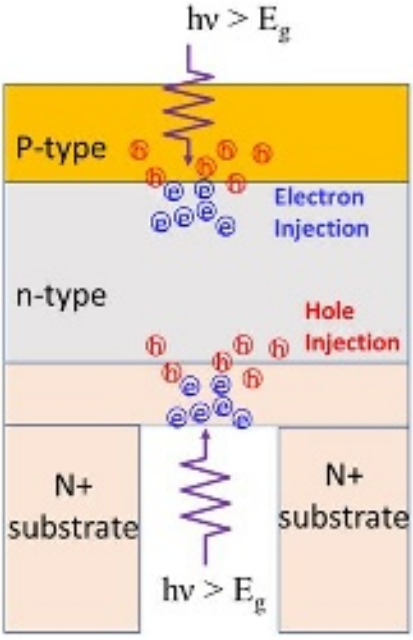
hν > E_g
P-type
Electron Injection
n-type
Hole Injection
N+ substrate
N+ substrate
hν > E_g

(a)

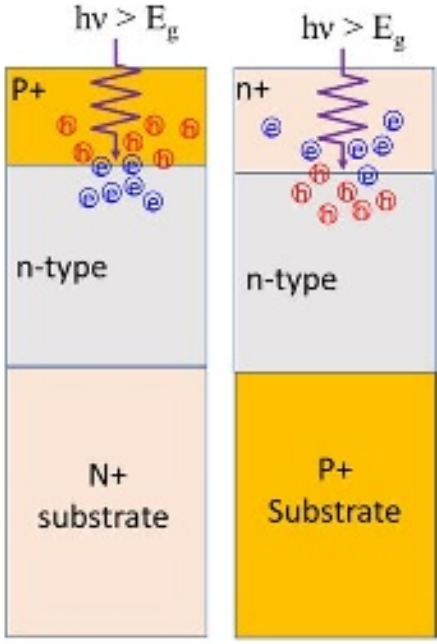
hν > E_g
hν > E_g
P+
n+
n-type
n-type
N+ substrate
P+ Substrate

(b)

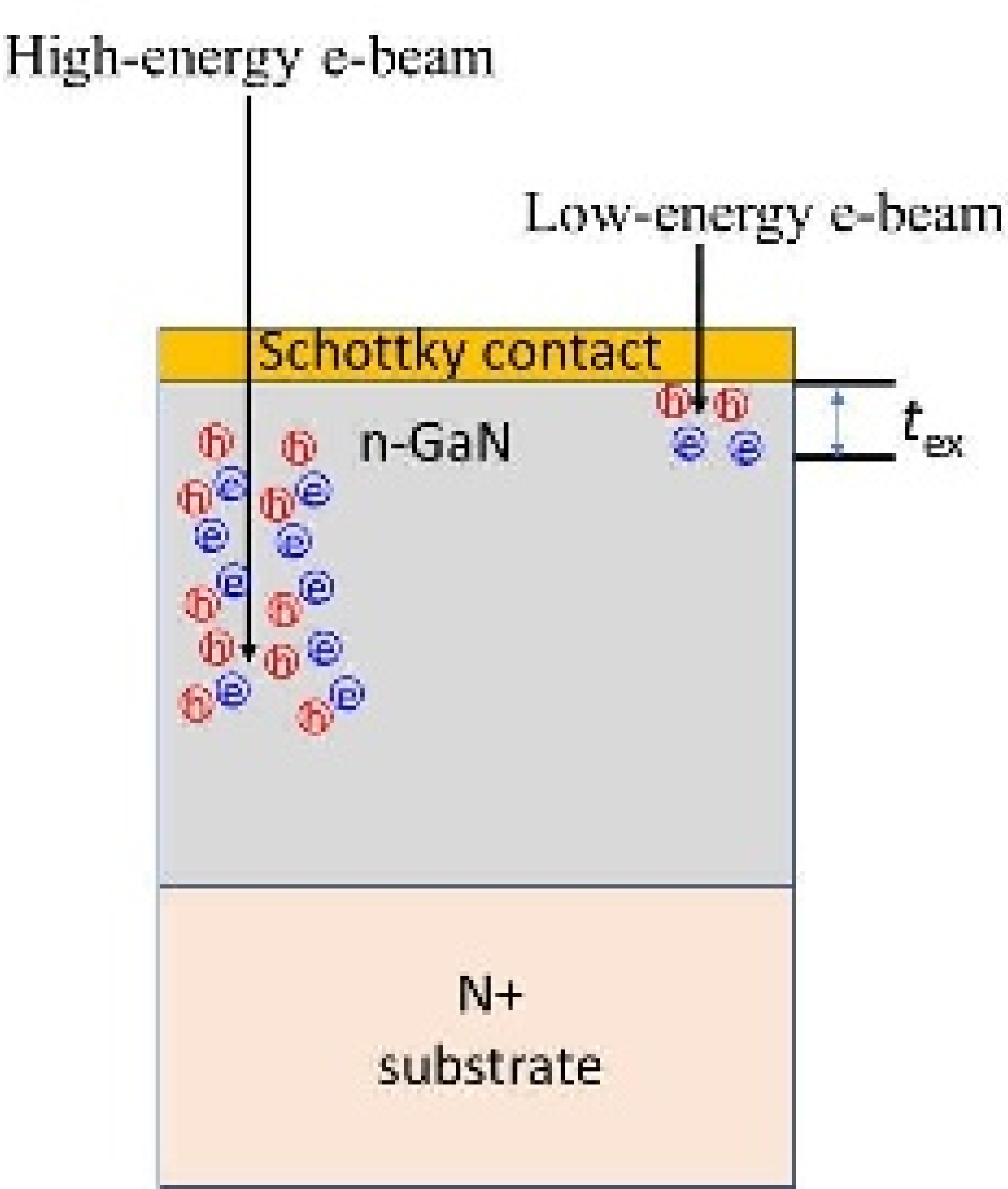
High-energy e-beam
Low-energy e-beam
Schottky contact
n-GaN
t_{ex}
N+
substrate

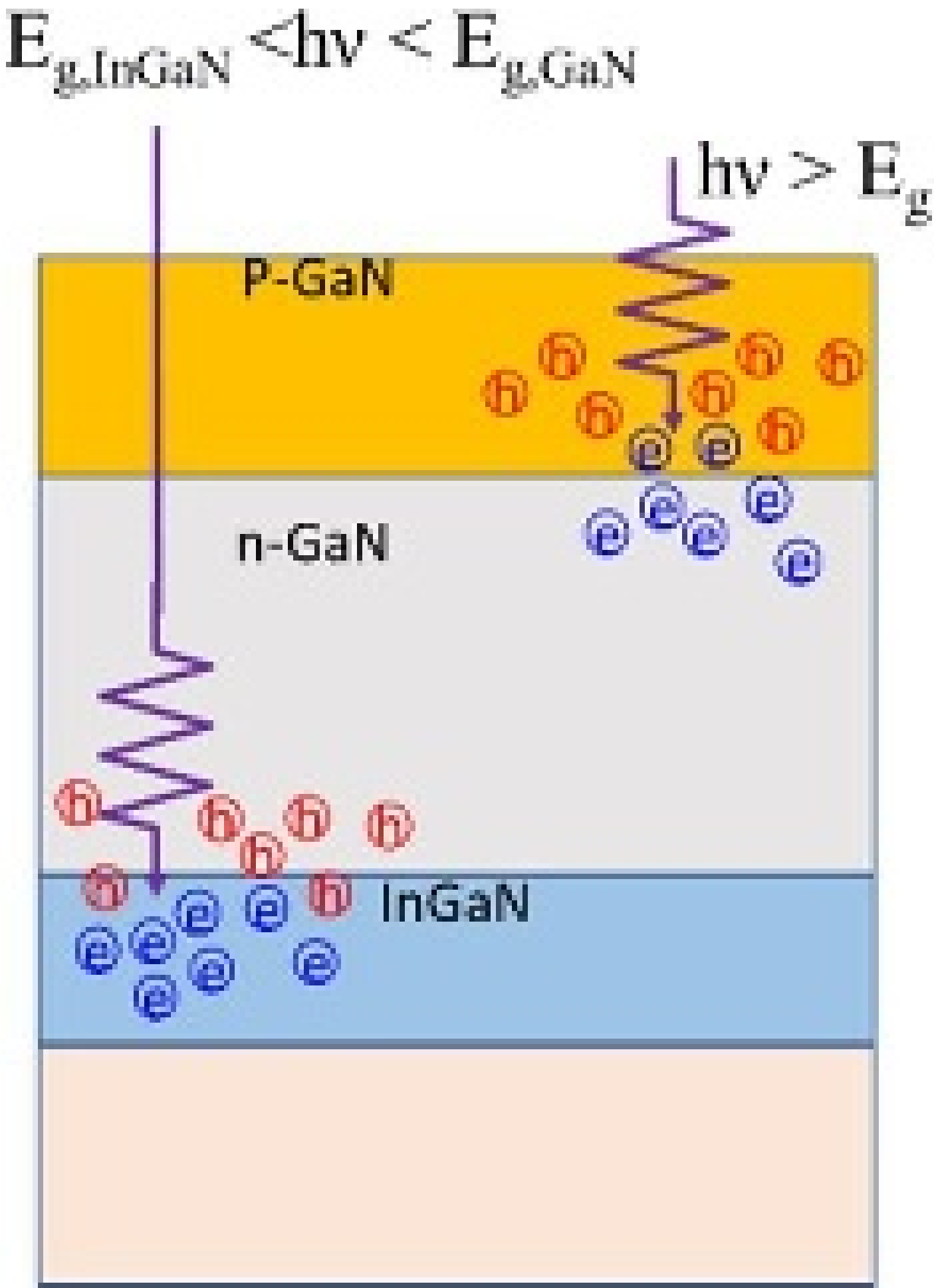
$E_{g,InGaN} < hv < E_{g,GaN}$
$hv > E_g$
P-GaN
n-GaN
InGaN

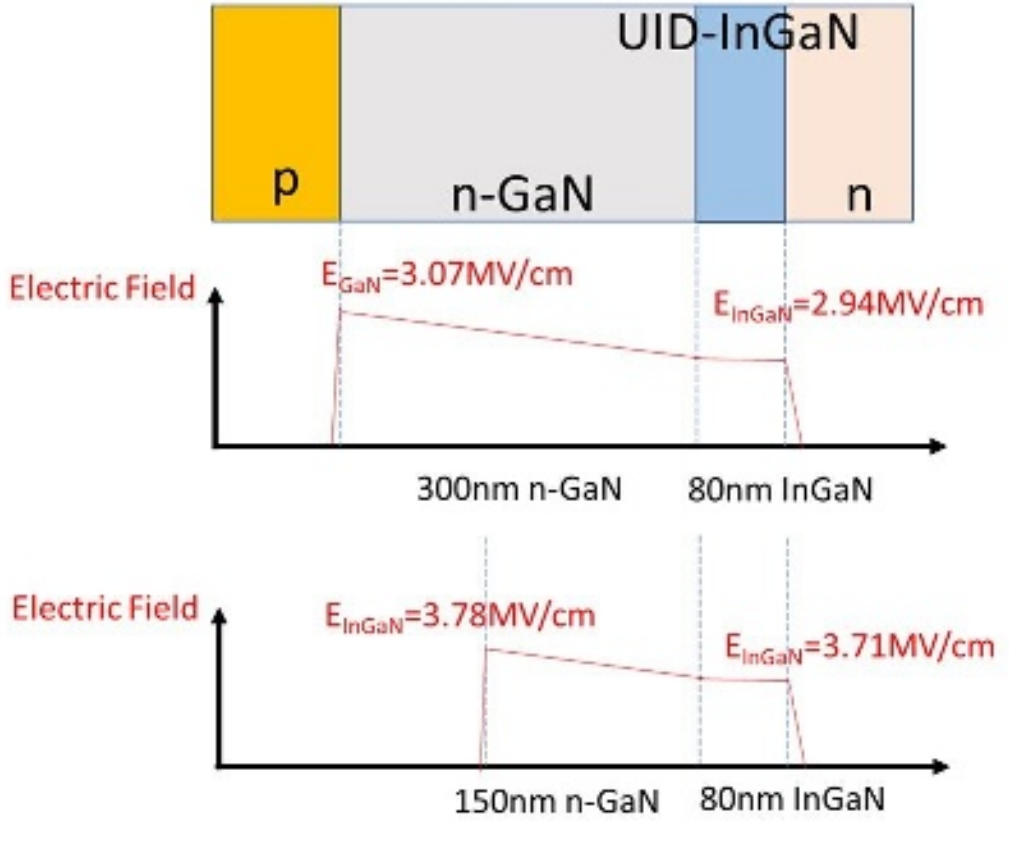
UID-InGaN
p
n-GaN
n
Electric Field
E_{GaN}=3.07MV/cm
E_{InGaN}=2.94MV/cm
300nm n-GaN
80nm InGaN
Electric Field
E_{InGaN}=3.78MV/cm
E_{InGaN}=3.71MV/cm
150nm n-GaN
80nm InGaN

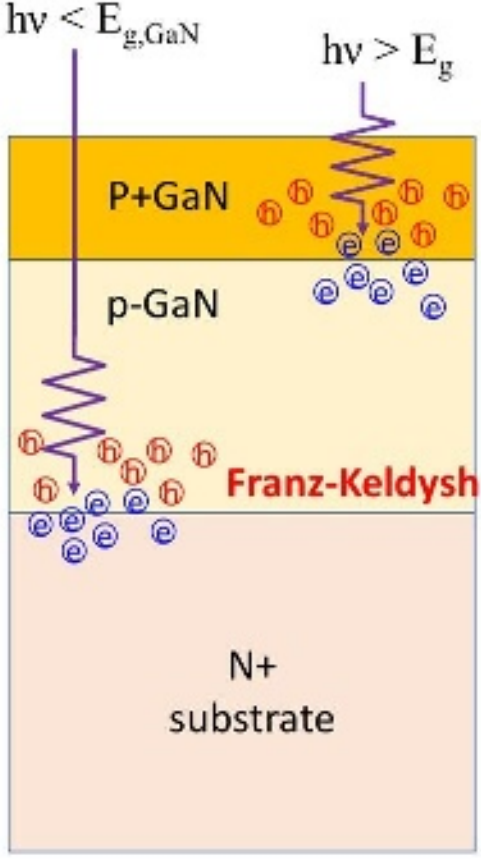
hν < E_g,GaN
hν > E_g
P+GaN
p-GaN
Franz-Keldysh
N+
substrate

(a)

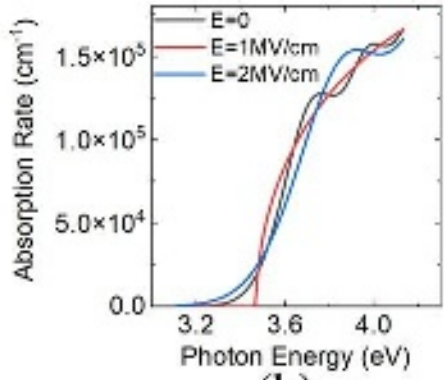
E=0
E=1MV/cm
E=2MV/cm
Absorption Rate (cm⁻¹)
1.5×10⁵
1.0×10⁵
5.0×10⁴
0.0
3.2
3.6
4.0
Photon Energy (eV)

(b)

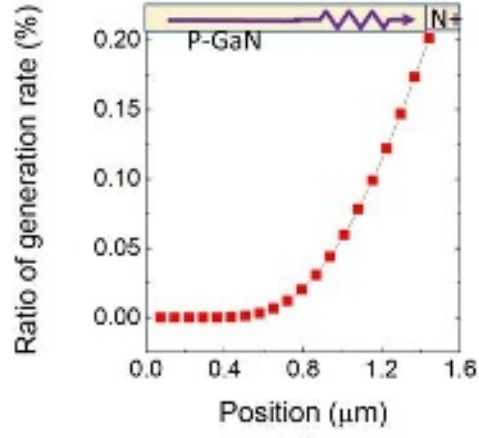
P-GaN
N+
Ratio of generation rate (%)
0.20
0.15
0.10
0.05
0.00
0.0
0.4
0.8
1.2
1.6
Position (μm)

(c)

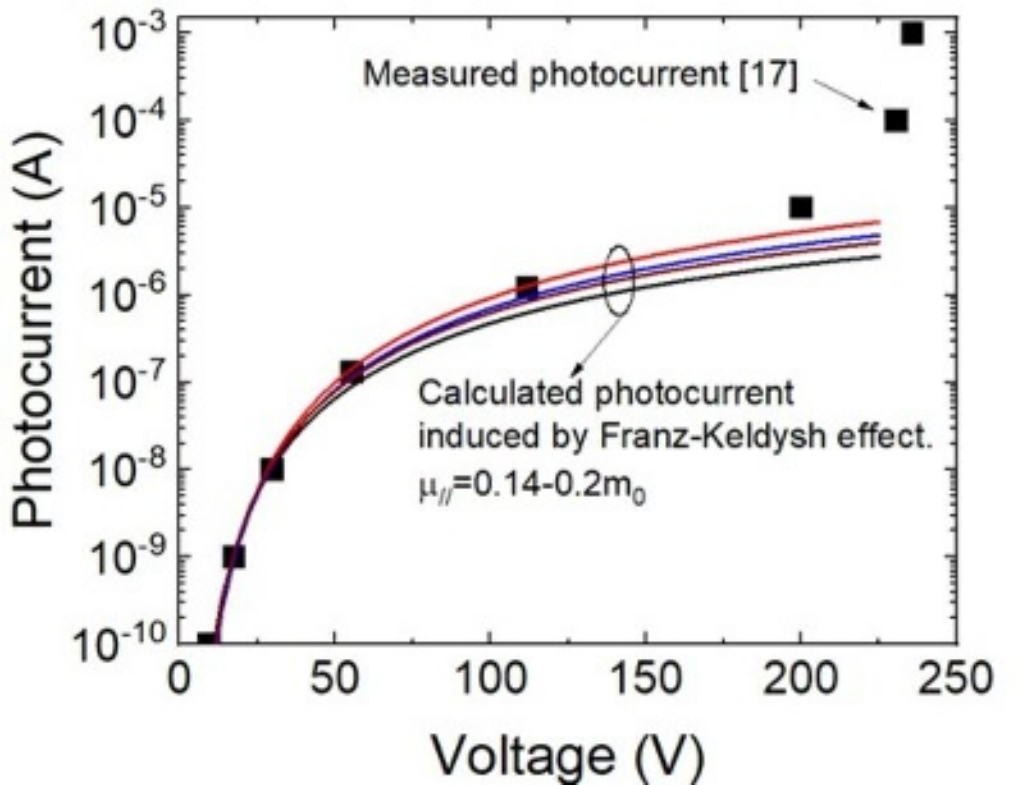
Measured photocurrent [17]
Calculated photocurrent
induced by Franz-Keldysh effect.
$\mu_{//}$=0.14-0.2m_0
Photocurrent (A)
Voltage (V)
10^{-3}
10^{-4}
10^{-5}
10^{-6}
10^{-7}
10^{-8}
10^{-9}
10^{-10}
0
50
100
150
200
250

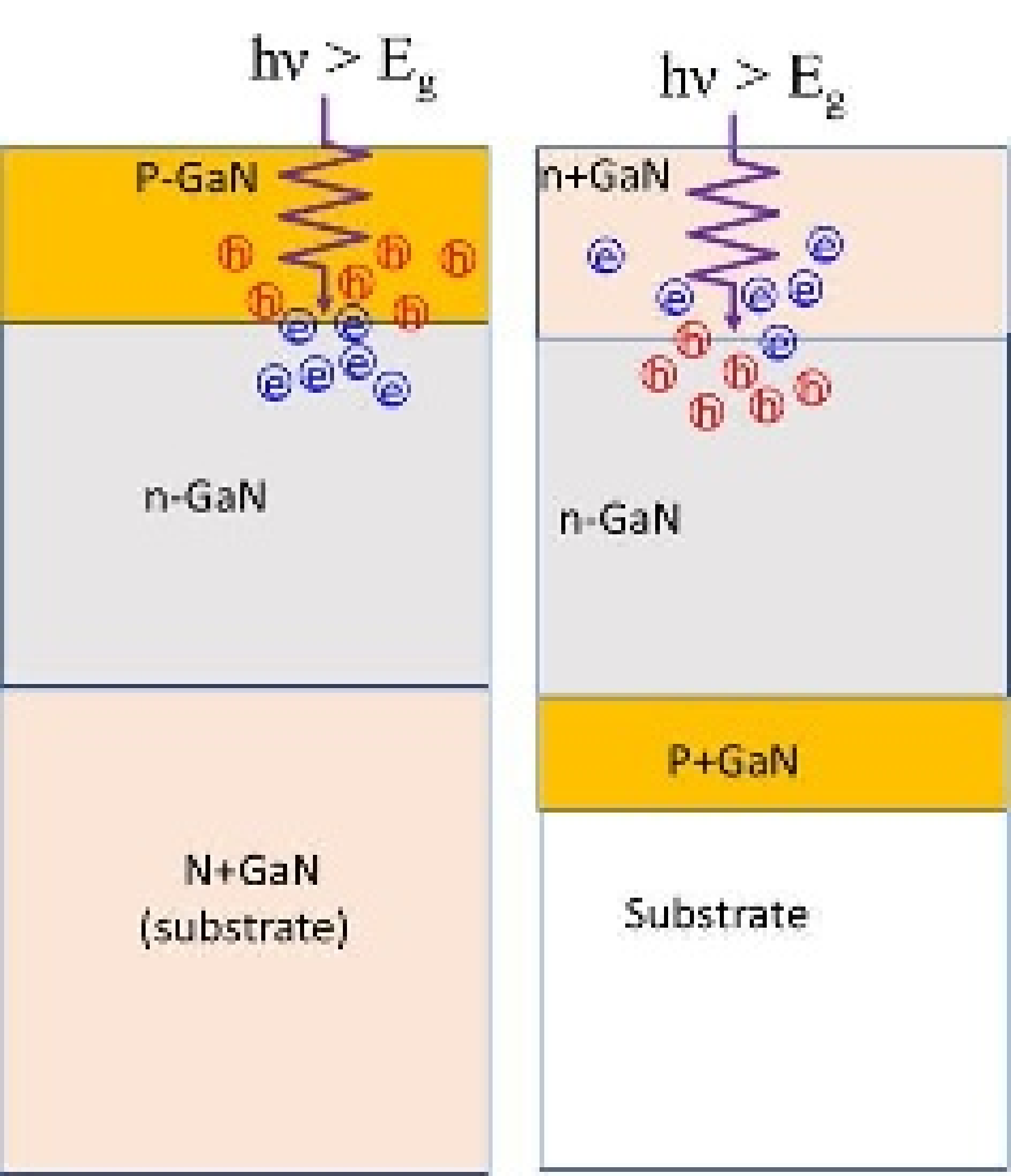
hv > Eg
P-GaN
n-GaN
N+GaN
(substrate)
hv > Eg
n+GaN
n-GaN
P+GaN
Substrate

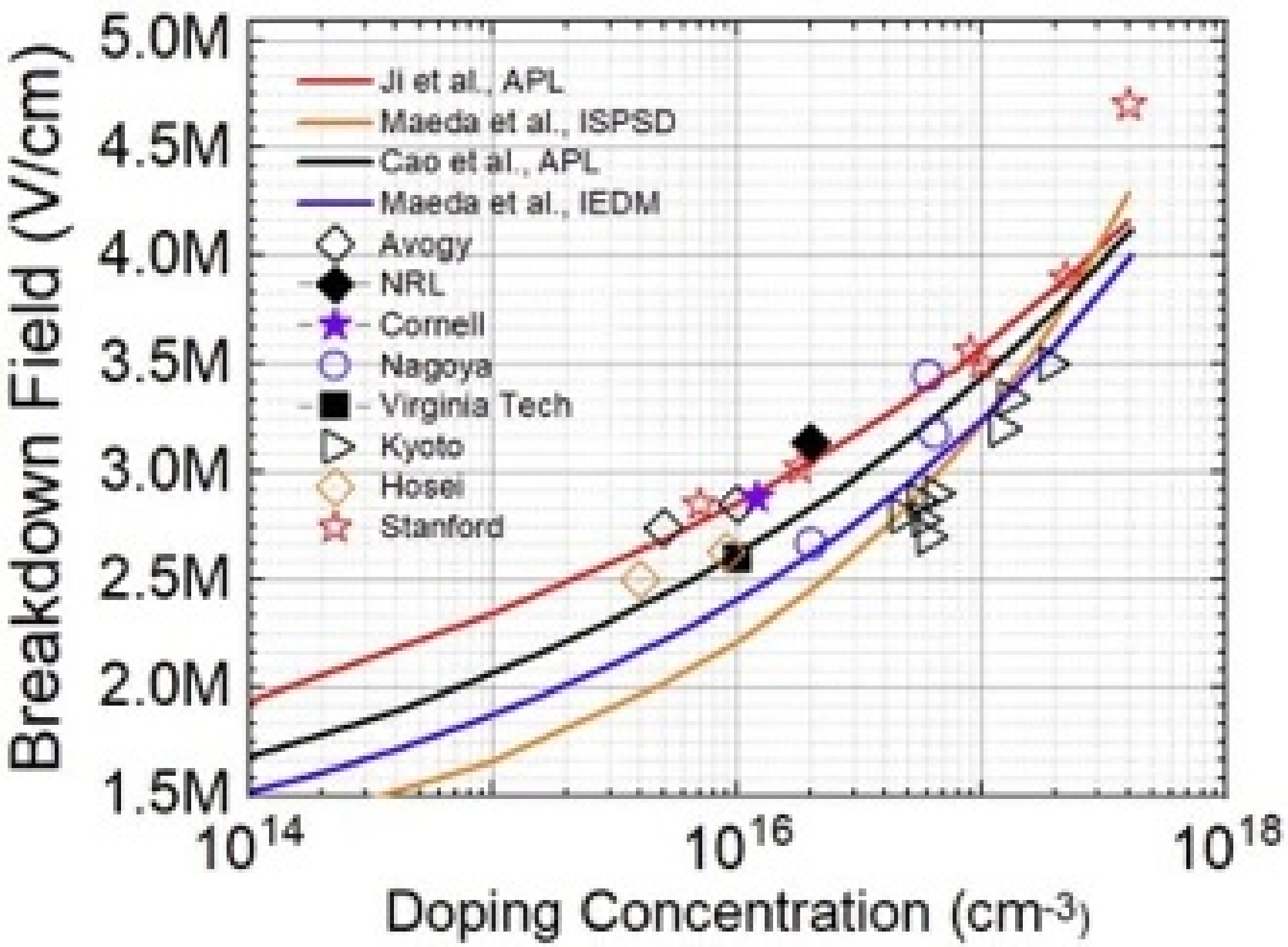
Breakdown Field (V/cm)
5.0M
4.5M
4.0M
3.5M
3.0M
2.5M
2.0M
1.5M
Ji et al., APL
Maeda et al., ISPSD
Cao et al., APL
Maeda et al., IEDM
Avogy
NRL
Cornell
Nagoya
Virginia Tech
Kyoto
Hosei
Stanford
10^{14}
10^{16}
10^{18}
Doping Concentration (cm^{-3})